THE ASTROPHYSICAL JOURNAL, 223:961–972, 1978 August 1

ORTHOGONAL MODES OF POLARIZATION FROM PULSAR PSR 2020+28

J. M. CORDES
Department of Physics and Astronomy, University of Massachusetts
JOANNA RANKIN
Astronomy Department and National Astronomy and Ionosphere Center, Cornell University
AND
D. C. BACKER
Radio Astronomy Laboratory, University of California, Berkeley
Received 1977 October 31; accepted 1978 February 9

ABSTRACT

Polarization at 430 MHz is studied over time scales from 8 μs to several years. We identify two orthogonal modes of polarization that have position angles separated by 90° and opposite senses of circular polarization. The correlation of position angle with sense of circular polarization is firmly established. The occurrence of the modes is studied as a function of pulse longitude and over pulse-to-pulse time scales. The intensity and frequency of occurrence of the modes show markedly different longitude distributions. At one longitude, switching between modes occurs in most pulses, while at another longitude where the modes are roughly equally probable, switching occurs stochastically from pulse to pulse and within single pulses on the periphery of subpulses. Switching is correlated with quasi-systematic intensity variations in one pulse component that occasionally appear as strong pulses alternated by weak pulses. One mode is clearly associated with a larger range of intensities than is the other mode; however, there is no evidence for a threshold intensity above which one mode is radiated and below which the other is radiated. We mention indications that average polarization profiles may change slightly on time scales of weeks to months.

Subject headings: polarization — pulsars

I. INTRODUCTION

Pulsars are noted for their highly polarized emission and for intensity variations with time scales ranging from microseconds (Hankins 1971) to months (Huguenin, Taylor, and Helfand 1973). A considerable body of literature exists which describes the phenomenology of pulsar polarization, some of which is understood within the context of the oblique rotator pulsar model (Radhakrishnan and Cooke 1969); however, many aspects of this phenomenology are not yet understood. Basically it is found that fluctuations of the state of polarization are strongly coupled to intensity variations (Cordes and Hankins 1977) and that they occur in at least three forms:

1. There is a slow variation with pulse longitude of the polarization of average pulse profiles. Nonmonotonic and discontinuous rotations of the polarization position angle are observed for some pulsars, but these can be attributed to the occurrence of orthogonal modes of polarization in single pulses. The relative strengths of the two modes vary with pulse longitude, thus causing discontinuities in the average position angle (Backer, Rankin, and Campbell 1976).

2. There are transitions between two orthogonal states of polarization; large intensity gradients are evidently necessary but not sufficient conditions for transitions to occur in single pulses. Transitions also occur from pulse to pulse. In several objects, the transitions are coupled to drifting subpulse patterns (Rankin, Campbell, and Backer 1974; Taylor *et al.* 1971).

3. There are erratic changes of the polarization state from pulse to pulse that more extensively depolarize synchronous averages at the higher frequencies, e.g., at least $\sim$1 GHz (Manchester, Taylor, and Huguenin 1975).

The position-angle variation in a given pulse is evidently determined by both a geometrical mechanism and a stochastic process describing the switching between orthogonal modes. The geometric aspect comprises the changing projection—due to stellar rotation—of some vector (e.g., the magnetic pole) onto the plane of the sky, a model that closely mimics the position-angle rotations observed from several pulsars (Radhakrishnan and Cooke 1969; Komesaroff 1970; Manchester and Taylor 1977). Orthogonal modes complicate the position-angle rotation in some average profiles, but each mode rotates with longitude in a fashion consistent with a geometric origin.

Transitions between orthogonal modes may be intrinsic to the emission process or may be imposed on radiation by propagation effects in the pulsar magnetosphere. If two orthogonal modes of polarization contribute to the initial radiation, the polarization observed may depend on the optical depths for absorption (Manchester, Taylor, and Huguenin 1975) or for

Thomson scattering (Blandford and Scharlemann 1976), which may differ in a time-variable fashion.

The present paper explores intensity and polarization variations from PSR 2020+28, the aim being to gain insight into the possible determinants of polarization transitions. We investigate polarization over the range of time scales from 8 μs to several years. Particular attention is devoted to correlations with intensity of the position angle. Orthogonal modes are described as accurately as possible in the hope that the underlying mechanism can be discerned. PSR 2020+28 was selected for detailed study because of its high polarization, both circular and linear, and because the modality phenomenon appeared to play a particularly constitutive role in its intrapulse structure.

II. OBSERVATIONS

Observations were made at Arecibo Observatory with the 305 m dish and the 430 MHz line feed which provides both senses of circular polarization. Instrumental polarization for this feed has been discussed in detail by Rankin, Campbell, and Spangler (1975) and Cordes and Hankins (1977). Cross-coupling of power between the two circular polarizations provided by the line feed has an upper limit of 0.25%. Cross-coupling conserves polarized power but linearly polarized power can be converted to circularly polarized power and vice versa; an upper limit on power that is converted in this way is 10%. After considering gain mismatches of the two receivers, we believe that instrumental effects produce errors in the Stokes parameters that are less than 10% and may be less than 5%.

Two observing programs with different polarimeters and analysis programs were used. Relevant instrumental details are given in Table 1. The first (program I) has been described by Rankin, Campbell, and Backer (1974). Briefly, it is a polarimetric study commenced in 1971 of both average profiles and single pulses of a number of pulsars with approximately one milliperiod resolution. The second program (II) involves study of single pulses from pulsars with microsecond time resolution, results of which have been reported by Hankins (1971, 1972, 1973), Cordes (1975, 1976*a*), Rickett, Hankins, and Cordes (1975), and Cordes and Hankins (1977). Program II involves sampling of signals before detection, application of a digital filter to remove the effects of interstellar dispersion, and subsequent formation of the Stokes parameters in the computer. Analysis includes formation of average profiles and computation of average autocorrelation functions of the Stokes parameters by summing autocorrelation functions of single-pulse Stokes parameters.

TABLE 1

DATA-ACQUISITION INFORMATION

Item	Program I	Program II
Dates	1972 June–present	1976 April, May
Bandwidth	500 kHz	125 kHz
Resolution		8 μs
Postdetection smoothing	0.33 ms/0°.35	0.26 ms/0°.27
Dispersion smearing	1.3 ms/1°.35	8 μs/0°.008
Polarimeter	Hardware, adding	Software

III. ORTHOGONAL MODES OF POLARIZATION

a) Single Pulses and Average Profiles

Figure 1 (Plate 34) shows the color-coded Stokes parameters of a sequence of 220 pulses obtained in program I. The total intensity (I), the percentage linear polarization [$100\,|L|/I$], the position angle [$\frac{1}{2}\tan^{-1}(U/Q)$], and the percentage circular polarization [$100\,V/I$] are plotted for a small range (28°.3) of pulse longitude centered on the expected arrival time of the pulses. Time extends from left to right through pulses and successive pulses are plotted from top to bottom.

The summation of 4400 pulses like those in Figure 1 yields the average polarization profile of Figure 2. The total intensity shows double-lobed structure that is common to many pulsars (Backer 1976); the intermediate "saddle" region is relatively broad compared with the widths of the lobes. Circular polarization is small except in component II, where it is about 10%. Linear polarization is a maximum in component I at 80% compared with 35% in component II. Most important, however, are the "nulls" in the linear polarization on the trailing edge of component I and on the leading edge of component II. The nulls align with rapid

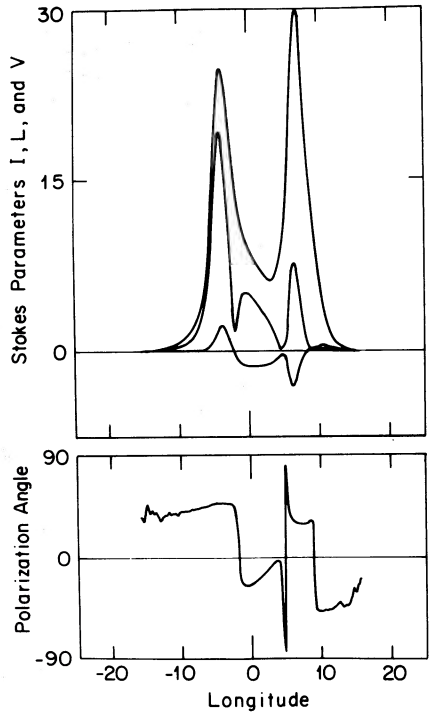

FIG. 2.—Average Stokes parameter profiles computed from 4400 pulses recorded on 1972 June 29. Resolution is 1.3 ms or 1°.35 of pulse longitude. Stokes parameters are expressed in Jy. Position angles are not absolute.

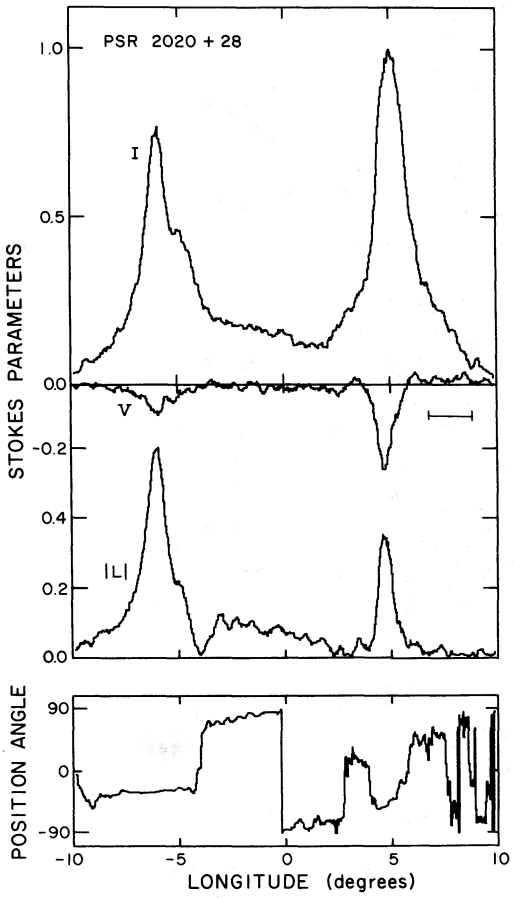

FIG. 3.—Average profiles of the Stokes parameters computed from 400 single pulses recorded on 1976 March 29. The horizontal bar represents 5 ms of intrapulse time. Resolution is 0.256 ms or 0°.27 of longitude. The position-angle scale is rotated by an arbitrary angle relative to position angles in Figs. 1, 2, 5, and 6. Note that the sense of circular polarization in component I is opposite that in Fig. 2.

swings of the polarization angle of approximately 90°. It is clear from Figure 1 that the first null and discontinuity of position angle occur in nearly every pulse. In component II the position angle usually rotates smoothly within a single pulse. Occasionally within single pulses and more often from pulse to pulse, however, the position angle jumps between orthogonal angles (orange and cyan).

Observations of PSR 2020+28 on a given day yield stable average polarization profiles if at least ~300 pulses are summed. Average profiles from different days may show significant differences, however. For example, the circular polarization in component I in Figure 2 is positive (LHCP). An average profile obtained on a different date (Fig. 3) has negative circular polarization (RHCP) in component I. We defer a discussion of such long-term variations until § V. In the remainder of this section we discuss short-term fluctuations of the total intensity and state of polarization.

The pulse intensities in Figure 1 are heavily modulated from pulse to pulse by both random variations and systematic patterns. The level of modulation is quantified by the intensity modulation index, defined by

$$m_I = (\sigma_I^2 - \sigma_{I\mathrm{off}}^2)^{1/2}/\langle I \rangle \qquad (1)$$

and plotted in Figure 4. The modulation index is smallest in the saddle region, implying a relative stability of the emission there. The modulation index is largest on the wings of the average profile where emission is only occasionally strong. Also displayed in Figure 4 is the frequency of occurrence of maximum emission as a function of longitude. The strongest emission usually occurs in narrow longitude regions centered on components I and II. In component I there appear to be two preferred locations for maximum emission that are apparently related to features in the modulation index. Moreover, these locations may be identifiable with subfeatures in component I that are evident in Figure 3.

Systematic pulse-to-pulse fluctuations are revealed by spectral analysis of the intensity at fixed longitudes. Backer, Rankin, and Campbell (1975) found patterns with characteristic periods of $P_3 \sim 3P_1$ in component I and $P_3 \sim 2P_1$ in component II (P_1 is the fundamental

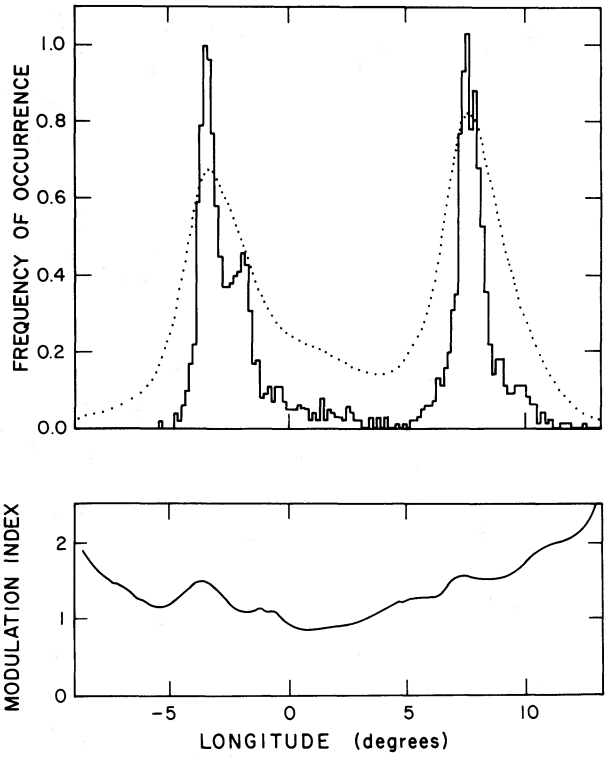

FIG. 4.—Histograms of the longitudes of maximum emission in single pulses superposed with the average profile. The histogram demonstrates that peak emission occurs within narrow ranges centered near the two lobes of the average profiles. Other pulsars sometimes show frequent strong emission in between the two average profile lobes. Also shown is the intensity modulation index.

pulse period). The relationship of polarization to systematic intensity variations will be discussed later in this section.

b) *Identification of Modes of Polarization*

The polarization of single pulses and average profiles suggests the presence of two preferred position angles at some pulse longitudes. To manifest the presence of these two position angles and the way their frequency of occurrence changes with longitude, histograms of the state of polarization are shown in Figure 5. For each longitude bin, histograms were computed of the position angle, the magnitude of the linear polarization, and the circular polarization of 1537 pulses.

Plotted symbols represent the fractional occurrence of quantities at each longitude bin. Outstanding features include: (1) a large fraction of nearly completely linearly polarized intensities at the peak of component I; the state of polarization is stable here with 80% linear polarization in the average profile; (2) the preference in component I for position angles to occur in a narrow range of values centered on about 52°; on the trailing edge of component I the histogram of angles itself jumps by 90°, indicating that a mode orthogonal to that which predominates in component I is preferred; consistent with the 90° jump is a null in the percentage linear polarization; and (3) a bimodal distribution of position angles beginning on the leading edge of component I and extending through component II.

The polarization histograms clarify the behavior of the average polarization in Figure 3. The discontinuities of the average position angle at longitudes of $-4°$, $+3°$, $+4°$, and $+6°$ are clearly due to the changes in the relative average contributions of the two polarization states.

c) *Isolation of Modes of Polarization*

Some interpretive comments on the histograms are in order here. The histograms clearly show the presence of two orthogonal position angles, but we note that the state of polarization at any instant may or may not derive solely from one or the other of the modes. Suppose the linear polarization $L = Q + iU$ is an

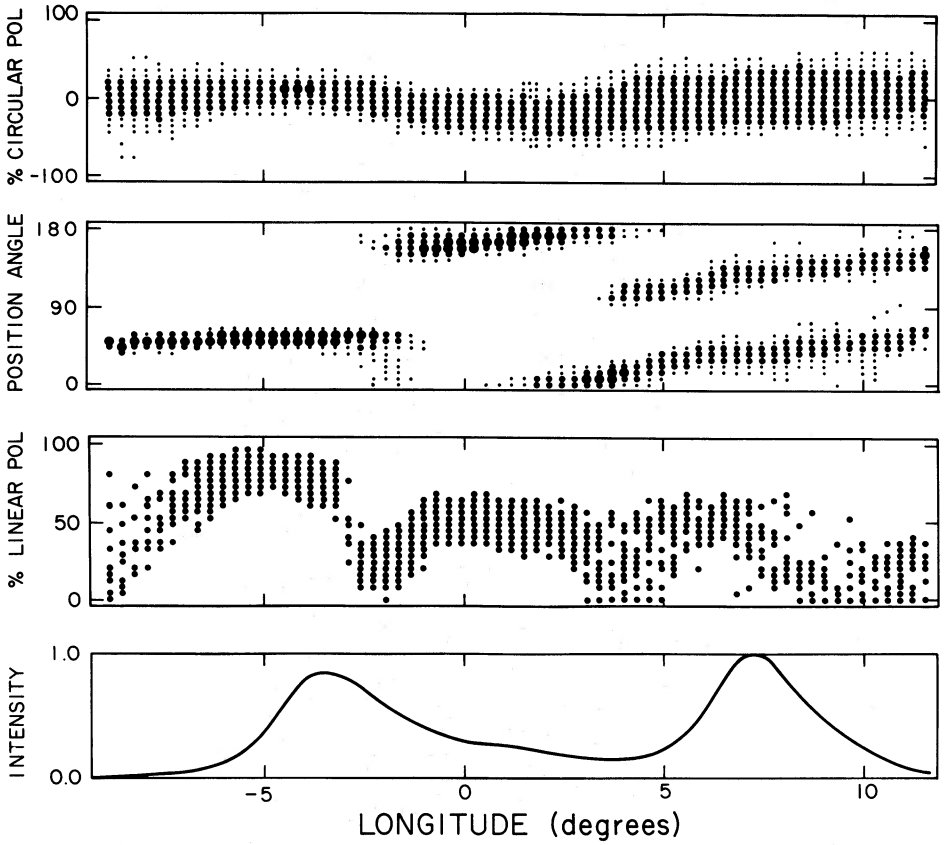

FIG. 5.—Histograms of the percentage linear and circular polarization and of the polarization position angle as functions of pulse longitude. Sizes of plotted circles are proportional to the fraction of pulses for which the quantities achieve their possible values. Small dots denote a fraction between 0.05% and 4.99%, medium-size dots a fraction between 5% and 35%, large dots a fraction between 35% and 70%. No fractions are larger than 80%. Fractions less than 0.05% are not plotted. For the percent linear polarization, fractions less than 5% also are not plotted; 1536 pulses from observations of 1972 June 29 were used. Data with intensities below a 3 Jy threshold were not used in the computation.

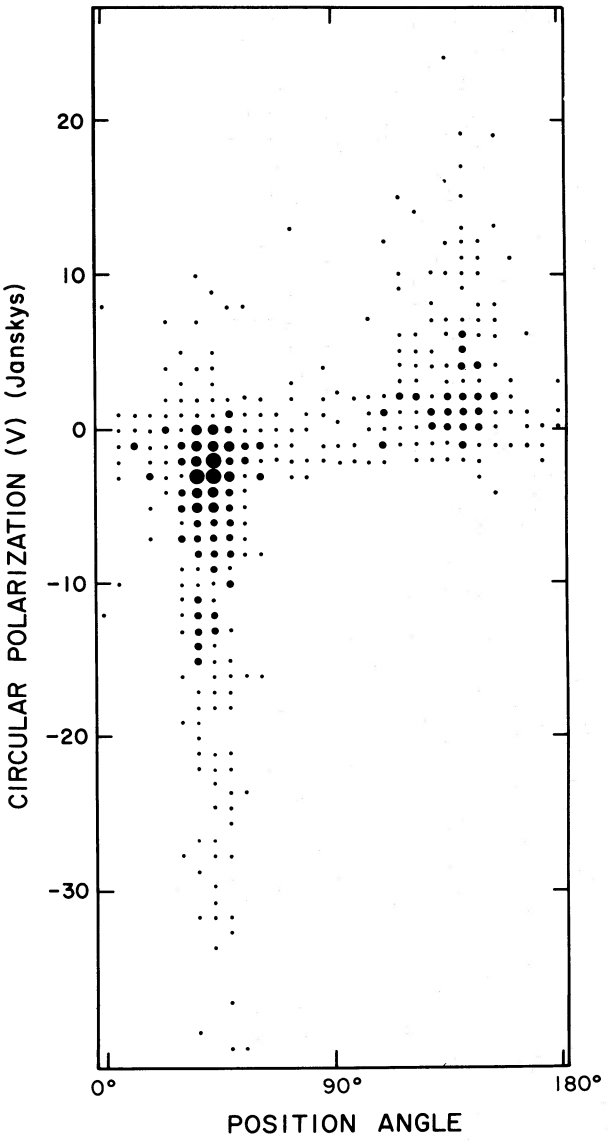

FIG. 6a

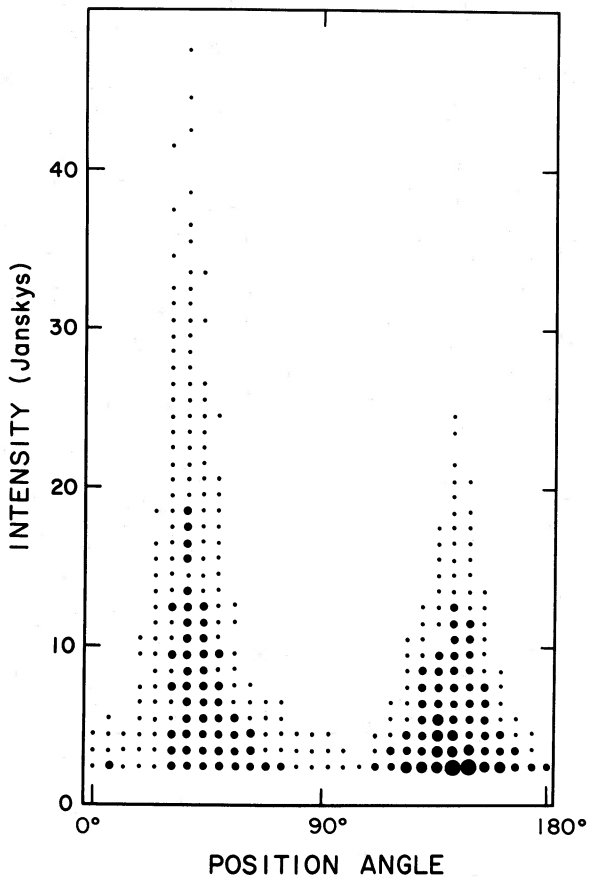

FIG. 6b

FIG. 6.—(*a*) Scatter plot of the Stokes parameter V versus the position angle for 2000 pulses observed on 1972 June 29. Samples used were those of maximum intensity occurring in component II of the average profile. Sizes of plotted circles are proportional to the number of pulses (out of 2000). The four sizes correspond to the ranges (from small to large) of: 1 to 3 pulses, 4 to 8 pulses, 9 to 15 pulses, and more than 15 pulses. (*b*) Similar scatter plot of total intensity versus the position angle. Intensities less than 2 Jy have not been included.

admixture of two modes, $L = L_1 + L_2$, where

$$L_1 = |L_1| \exp(2i\psi)$$

$$L_2 = |L_2| \exp[2i(\psi + \pi/2)] = -|L_2| \exp(2i\psi) . \quad (2)$$

Apart from a phase factor ($e^{2i\psi}$), one mode has positive real linear polarization, the other has negative real linear polarization; i.e., the vectors L_1 and L_2 are antiparallel on the complex plane and therefore the net position angle is determined by the larger of $|L_1|$ and $|L_2|$. In this idealized situation, intermediate position angles between ψ and $\psi + (\pi/2)$ do not occur for the sum $L = L_1 + L_2$. Therefore, unless the radiation at any instant is exclusively of one mode, the histograms of position angle measure only how often one mode *dominates* the other, rather than how often each mode occurs.

Luckily, it appears that modes occur disjointly (i.e., only one mode contributes to the emission at any instant) for PSR 2020+28 for the most part, as we shall demonstrate. First, in Figure 6*a*, we show a scatter plot of Stokes parameter V (circular polarization) and position angle for a range of longitude that

encloses component II of the average profile. Clearly, negative values of V (RHCP) are associated with one position angle (mode 1), positive values with the other position angle. The precision of this relationship can be determined from the correlation coefficient

$$\rho_{lv} \equiv |\langle lv \rangle| \equiv |\langle \mathrm{sgn}\,[\mathrm{Re}\,(L)]\,\mathrm{sgn}\,V \rangle|\,, \qquad (3)$$

where $\mathrm{sgn}\,(x) = \pm 1$ for $x \lesseqgtr 0$. We presume, in the case of the pulsar emission, that the position angles of the modes are rotated such that L is real and is either positive or negative. For random noise, $\rho_{lv} = 0$ because Re (L) and V are independent and are equally likely to be positive and negative. When the signs of L and V are deterministically related, $\rho_{lv} = 1$. From the data used to form the scatter plot of Figure 6*a*, we obtain $\rho_{lv} = 0.97$. Only those values of V were used whose magnitudes were greater than twice the standard deviation of the off-pulse V. A value of ρ_{lv} so close to unity implies one of several possibilities: (*a*) modes occur disjointly; (*b*) modes are superposed and are of comparable intensity but at any instant one mode is always more strongly polarized (both linearly and circularly); or (*c*) the intensity in one mode is instantaneously larger than that of the other, so that fluctuations in the degree of polarization do not destroy the relationship between L and V.

Additional criteria, besides the correlation of the signs of V and L, for deciding whether modes occur disjointly are: (1) There is a large average fractional linear polarization. The net average fractional linear polarization,

$$\langle d_L \rangle = [|\langle L_1 \rangle| - |\langle L_2 \rangle|]/\langle I_1 + I_2 \rangle\,, \qquad (4)$$

is clearly lessened if both modes contribute at a given pulse longitude. (2) A large second moment of d_L will denote large instantaneous linear polarization even though the average d_L may be small. We write

$$\langle d_L^2 \rangle \equiv \frac{\langle |L|^2 \rangle}{\langle I^2 \rangle}$$

$$= \frac{\langle L_1^2 \rangle + \langle L_2^2 \rangle}{\langle (I_1 + I_2)^2 \rangle} \quad \text{(disjoint)}$$

$$= \frac{\langle L_1^2 \rangle + \langle L_2^2 \rangle - 2|\langle L_1 \rangle||\langle L_2 \rangle|}{\langle (I_1 + I_2)^2 \rangle}\,,$$

(superposition) (5)

where the cross term, $-2|\langle L_1 \rangle||\langle L_2 \rangle|$, is absent when the modes occur disjointly and it is assumed that both modes occur equally frequently when they are disjoint. As an extreme example, the mean value of d_L could be zero while the mean-square value is unity if the modes are disjoint; if the modes superpose, then the mean-square value can be zero as well.

Both criteria are satisfied in component I of the average profile of PSR 2020+28 where the mean degree of linear polarization is 78% and the mean-square value is 80%. The depolarization may be due to emission in the other mode (mode 1) whose contribution to the intensity is one-ninth that of mode 2 if mode 1 is 100% polarized or is one-fourth the intensity of mode 2 if mode 1 is unpolarized. It seems unlikely that more than one mode contributes because the degree of polarization is fairly steady from one pulse to the next.

Saddle region emission is typically more than 50% linearly polarized with the position angle nearly always being 90° away from that in component I. If both modes contributed, one might expect occasional sign changes in L due to random fluctuations in the relative strength of the two modes.

d) Relationship of Total Intensity to Mode of Polarization

The instantaneous mode of polarization is correlated with the total intensity, a result that also is consistent with disjoint occurrence of the modes. This is evident in Figure 1, where large intensities in component II usually have position angles of $\sim +30°$ (cyan), while $-60°$ position angles (orange) are preferred for diminished intensities. It is also clear that the instantaneous mode is synchronized with the previously mentioned systematic modulation of the intensity. The intensity is large every other pulse period and weak in between for 10 to 20 pulse periods, after which it becomes disorganized for 5 to 20 periods. Mode 1 tends to occur at the maxima of strong pulses; mode 2 is found on the trailing edges of the strong pulses and in the weak pulses. In this regard, PSR 2020+28 is similar to PSR 2303+30, which shows highly organized modulations on alternate pulse periods of the total intensity and state of polarization (Rankin, Campbell, and Backer 1974).

The state of polarization is determined precisely by neither the intensity relative to some local maximum (e.g., the maximum subpulse intensity) nor by the absolute intensity. This is clear from Figure 6*b*, where we show a scatter plot of intensity and position angle for the point of maximum intensity in component II in each of 2000 pulses. The effects of interstellar scintillation, which modulate the intensity on $\sim$1000 pulse time scales, were reduced by computing scatter plots for 200-pulse blocks and normalizing to the mean pulse intensity of that block. Clearly, small intensities (down to the 2 Jy noise limit) are associated with mode 1 as well as the largest intensities. Thus there is no detectable absolute intensity threshold above which one mode is preferred and below which the other is preferred. Furthermore, the fact that peak subpulse emission can occur in either mode implies that the radiated mode is not determined exclusively by the subpulse structure either. The strongest statement is that mode 1 occurs with a larger range of intensities than does mode 2.

e) Quantitative Separation of the Modes

Average profiles of the intensity, linear polarization, circular polarization, and frequency of occurrence can be made for radiation that is dominated by mode 1 and radiation that is dominated by mode 2. Moreover, if

we believe that the modes occur disjointly, then such profiles are of quantities associated with only one mode or the other. For each longitude bin of 1000 pulses, the position angle was determined and assigned to either mode 1 or mode 2. Correspondingly, I, the magnitude of L, V, and the number count were added to accumulators for the assigned mode. In Figure 7 we show the resultant integrated L, V, and frequency of occurrence for the two modes. The linear polarization profiles are markedly different, with mode 2 accounting for virtually all linearly polarized emission in component I and mode 1 accounting for all that in the saddle region. The integrated linear polarization and circular polarization are roughly proportional to the intensity of each mode. On the trailing edge of component I, mode 2 gets weaker with increasing longitude while mode 1 gets stronger. The longitude where the integrated linear polarization in the two modes is equal coincides with the notch in the total integrated linear polarization of Figures 2 and 3.

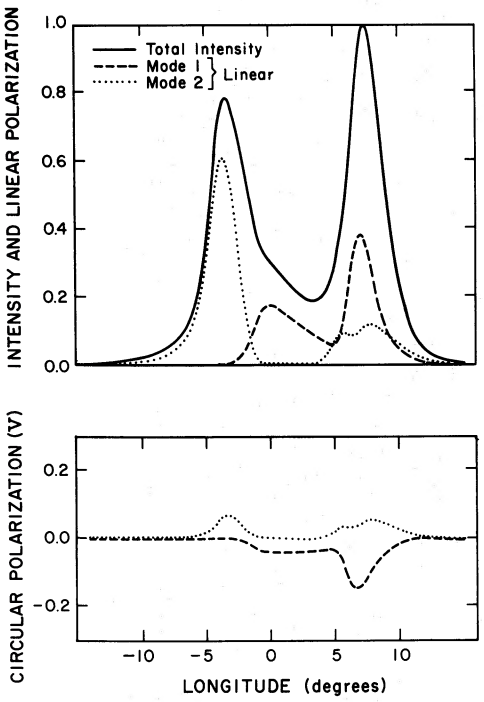

FIG. 7a

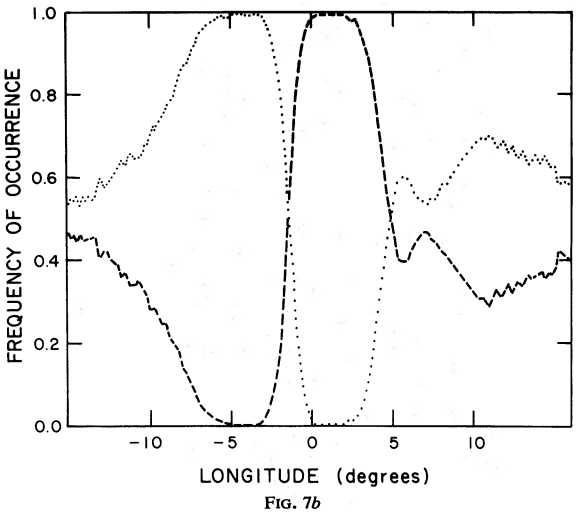

FIG. 7b

FIG. 7.—(*a*) Average profiles of the total intensity and of the linear and circular polarization of each of the orthogonal modes (see text). Data are from 1972 June 29. (*b*) The frequency of occurrence of the two modes as a function of longitude.

The integrated intensities tell nothing of the relative intensities of the two modes in single pulses. The frequencies of occurrence in Figure 7*b* show the fraction of position angles that are associated with each mode; the sum of the frequencies therefore equals unity. On the extreme left and right sides of the figure—i.e., where there is little pulsar emission—the frequency of occurrence becomes nearly equal to 0.5 for both modes because the position angle is determined mostly by off-pulse noise and is therefore uniformly distributed over 180°. The important portion of the figure is that corresponding to component II (longitudes 5° to 10°) where both modes undoubtedly contribute. Mode 2 occurs slightly more frequently than mode 1 (55% of the time). Therefore, the intensities in single pulses themselves are stronger, on average, for mode 1 because the integrated intensity is larger in mode 1 and single pulses occur less frequently in that mode.

Quantitatively, we can state that in component I, mode 2 dominates the emission at least ~99% of the time while mode 1 dominates saddle region emission at least ~99% of the time. In component II, 78% of the intensity and 45% of the pulses are dominated by mode 1; average intensity of mode 1 in single subpulses is about 4 times the average intensity of mode 2.

IV. POLARIZATION VARIATIONS ON MILLISECOND TIME SCALES

a) Autocorrelation Analysis

The study of polarization variations on short time scales within single pulses is best done by forming autocorrelation functions (ACFs) of the Stokes parameters of single pulses and summing them to form averages. Details of this processing have been discussed by Cordes (1976*b*) and Cordes and Hankins (1977). Briefly, we form average ACFs of I, V, and $L = Q + iU$ according to (e.g.)

$$R_L(\tau) = \sum_k \sum_t L_k(t) L_k^*(t + \tau) , \qquad (6)$$

where the asterisk denotes complex conjugation, the sum over k is a sum over pulses, and the sum over t is over time (longitude) within a single pulse. Similar ACFs are defined for I and V and normalized ACFs $r_I(t)$, $r_V(t)$, and $r_L(t)$ are formed by dividing all ACFs by $R_I(0)$. ACFs are computed separately for components I and II and the saddle region and are shown in Figure 8.

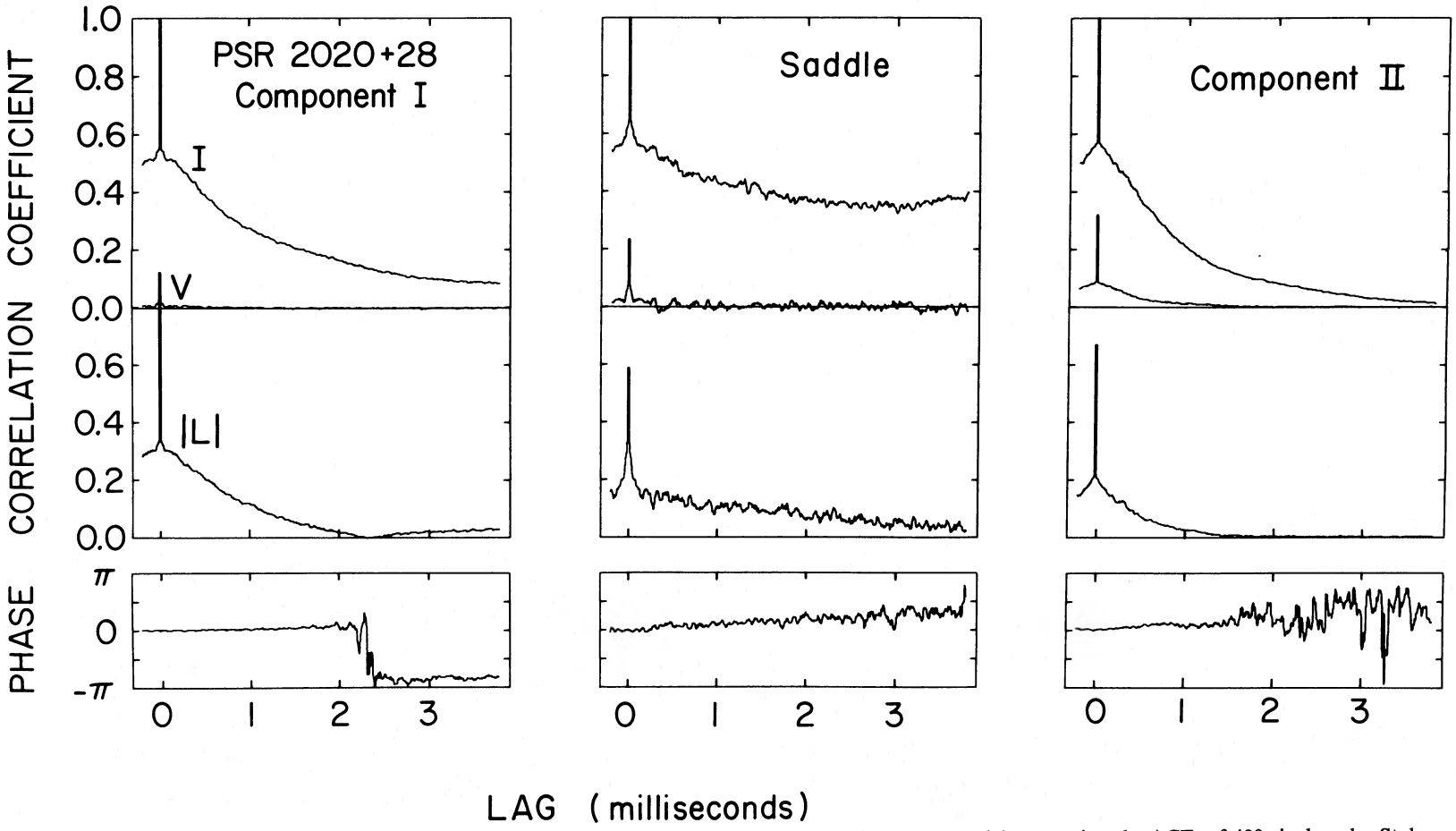

FIG. 8.—Autocorrelation functions (ACFs) of the Stokes parameters for three longitude regions computed by summing the ACFs of 400 single-pulse Stokes parameters obtained from data of 1976 March 29. The ACFs of the total intensity (I) and the circular polarization (V) are real, whereas the ACF of the linear polarization ($L = Q + iU$), for which we show the magnitude and phase, is complex. Except for the zero-lag spikes, the ACFs are smoothed over 40 μs.

Basically, the ACFs measure how the intensity and polarization decorrelate in time. Features in single pulses have characteristic time scales which can be identified in the ACFs. Cordes and Hankins (1977) have shown that polarization fluctuations are strongly coupled to the intensity variations. A simple empirical model (Cordes 1976*b*) shows that the ACFs of V and L can be expressed as

$$r_V(\tau) = R_{d_V}(\tau) r_I(\tau) , \quad (7)$$

$$r_L(\tau) = R_{d_L}(\tau) r_I(\tau) \exp(i\phi_L) , \quad (8)$$

where ϕ_L is the angle of the ACF of L in the complex plane, and R_{d_V} and R_{d_L} are the ACFs of the degree of circular and linear polarization defined as

$$d_V(t) = V(t)/I(t) , \quad (9)$$

$$d_L(t) = |L(t)|/I(t) . \quad (10)$$

Values of the ACFs near zero lag yield estimates of the mean-square degree of polarization, while the shapes of the ACFs, in comparison with that of the ACF of the total intensity, show the manner in which the polarization changes on different time scales.

The mean-square degree of linear polarization and circular polarization can be evaluated from the ACFs from

$$\langle d_L^2 \rangle = |r_L(0^+)|/r_I(0^+) , \quad (11)$$

$$\langle d_V^2 \rangle = r_V(0^+)/r_I(0^+) , \quad (12)$$

where $\tau = 0^+$ denotes a lag where the "zero-lag spikes" no longer contribute to the ACFs; the zero-lag spike has a height proportional to the variance of the correlated quantity and its width is equal to the reciprocal of the receiver bandwidth, 8 μs.

b) Results

The finest structure in single pulses consists of micropulses with $\sim$100 μs widths that occasionally occur in components I and II. Small signal-to-noise ratios in the saddle region prohibit direct observation of micropulses there. ACFs in Figure 8 for component I and the saddle region show narrow features with $\sim$100 μs widths that are due to microstructure. Broad features with $\sim$0.8 ms widths (half-widths at half-maximum) in component I and II are indicative of subpulse widths, although in component II there is no distinguishing manifestation (e.g., a break point in the autocorrelation functions) that micropulses (which *are* seen in single pulses) and subpulses are separate constituents. Indeed, the absence of a break point in the ACF for component II indicates either a continuum of time scales or that the short 100 μs micropulses contribute negligibly to the intensity second moment.

In Table 2 we list the mean values and rms values of d_L and d_V along with characteristic time scales that have been obtained from the ACFs.

In component I, the rms and the mean degree of linear polarization are nearly equal, signifying that there is little variation in d_L from pulse to pulse. More notable, however, is the zero crossing of the ACF of L at a lag of $\sim$2.3 ms, as indicated by the 180° jump in phase. This zero crossing is a consequence of the 90° jumps in the position angle that occur on the trailing edge of component I. The appearance of the zero crossing in the ACF of L is further indication that 90° jumps occur in many if not in all single pulses; the lag at which the zero crossing occurs is somewhat arbitrary because it depends on the region of longitude used to compute lagged products for the ACF.

ACFs for component II suggest that switching between orthogonal modes of polarization occurs in a significant fraction of single pulses and thereby causes V and L to decorrelate faster than the total intensity. ACFs of V and L have 0.36 ms widths, which are one-half the width of the ACF of the total intensity. This suggests that switching occurs on some characteristic time scale $\sim$0.36 ms. However, it appears that prior to or after a switch, the state of polarization is primarily in one mode or the other. This follows because the linear polarization and circular polarization have rms values of 61% and 39% compared with respective mean values of 38% and 25%. As discussed in a previous section, a difference between the rms and mean values is consistent with the two modes occurring disjointly rather than the instantaneous state of polarization being a linear sum of the two modes.

V. LONG-TERM VARIATIONS OF POLARIZATION

Variations in the morphological properties of pulsar total intensity average profiles are a well-known phenomenon. Helfand, Manchester, and Taylor (1975) have

TABLE 2

POLARIZATION PROPERTIES OF PSR 2020+28 AT 430 MHz*

AVERAGE PROFILE COMPONENT	$\langle d_L \rangle$	$\langle d_V \rangle$	$d_{L\,\mathrm{rms}}$	$d_{V\,\mathrm{rms}}$	ACF HALF-WIDTHS W_I (ms)	W_V (ms)	W_L (ms)
Component I.....	0.78	−0.10	0.80	0.20	0.76	...	0.76
Saddle.....	0.65	−0.1 to 0	...	...	...	...	...
Component II.....	0.38	−0.25	0.61	0.39	0.72	0.36	0.36

* Data used here refer to those appearing in Figs. 3 and 8; quantities can vary considerably from observation to observation, as discussed in text.

examined the problem in a general way and have shown, among other things, that pulsars like PSR 2020+28 with a complex profile require much longer averages to achieve a given level of stability than those either with simple profiles or with drifting subpulses. While Helfand *et al.* did not specifically consider PSR 2020+28, it nonetheless is in no way surprising to find that its average profile exhibits significant changes both from day to day and in separate averages of a few hundred pulses on a given day: the widths of the respective components, the minimum intensity of the saddle region, and the intensity ratio of the two components, for instance, vary by up to several tens of percent in successive average profiles.

We find, however, a further class of morphological variations whose contrasting properties compel us to note them here. Measures in this class do not typically vary inordinately in successive averages within a given day but are found to vary over intervals of weeks or months. A number of such quantities are plotted in Figure 9*a* as a function of time over the 2½ year period during which observations were carried out; they are the maximum fractional linear and circular polarization in components I and II, respectively: d_{L_I}, $d_{L_{II}}$, d_{V_I}, and $d_{V_{II}}$. As can be clearly seen, the quantities all show some mutual correlation.

The magnitude of long-term variations in the fractional polarization ranges upward to 30% and it remains to argue that such variations are significant. As discussed above, specification errors in the measured polarization can result either from (*a*) incorrect relative gain normalization between the two circular channels resulting in spurious V, or (*b*) cross-coupling of circularly and linearly polarized power. The latter consideration is of issue only in component I, where a 10% cross-coupling of the 75% linearly polarized signal results in a possible error in the circular, d_{V_I}, of some 7%, much less, however, than the

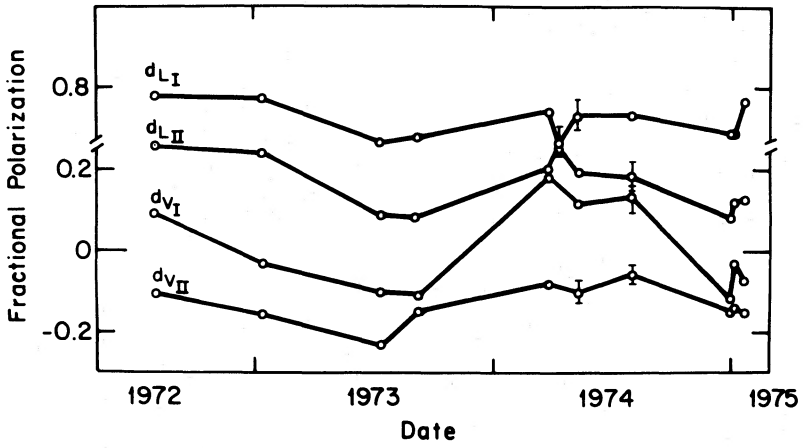

FIG. 9*a*

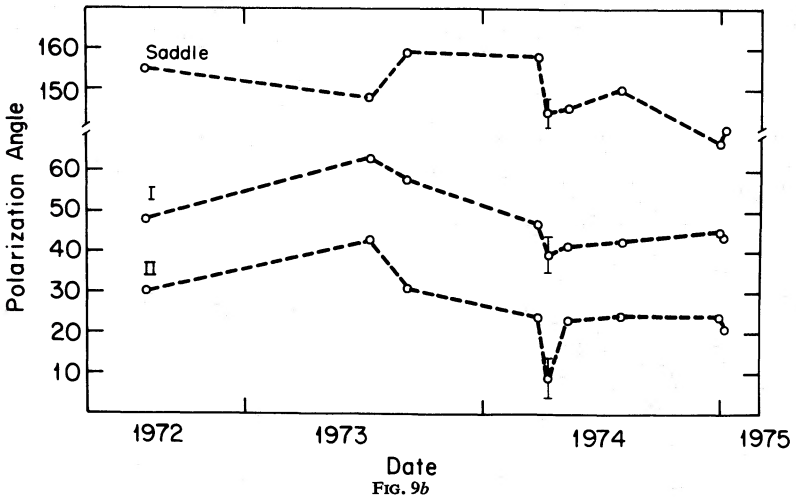

FIG. 9*b*

FIG. 9.—(*a*) Fractional polarization, both linear and circular, in each of the two pulse components of PSR 2020+28 over a 2½ year period. The observations were made with program I, of which Fig. 2 is typical. (*b*) Polarization angle in each of the two components and the saddle region as above.

30% variations observed. That the circular power and linear power are not obviously negatively correlated is further evidence that cross-coupling is not an important issue. The former matter is equivalent to ensuring that unpolarized signals acquire no spurious circular polarization in the course of our observing program. We note, however, that there is a point at about longitude 5° in Figure 3 which exhibits no more than about 4% circular polarization, and a further examination confirms that this was no less true for the 10 or more other observations made with program I. Thus improper gain normalization must introduce less than about 4% error in the specification of the fractional circular polarization—which again is much less than the scale of variations observed.

We note in passing that the polarization angles measured at the peak of the linearly polarized emission in components I and II and in the saddle region are relatively stable over intervals of several years. These measurements are plotted in Figure 9*b*. The principal source of error is Faraday rotation in the Earth's ionosphere which can be specified only to perhaps ±5°. The polarization angle in components I and II is generally compatible with 44° ± 5° and 26° ± 5°, respectively; the discrepant points in late 1973 are perhaps noteworthy. The angle in the saddle region is about 147° ± 5°.

If the variations considered by Helfand *et al.* in the total intensity profile are related to the pulsar beam mechanism, the issues of concern here are more relevant to the pulsar radiation mechanism, an emission mechanism which is undergoing a slow evolution, assuming a number of different stable states, or being shifted spacially (perhaps through precession?) to reveal different aspects of its lobe structure. Some of the variations in question, particularly the change in the amount and form of the linear polarization in component II, may be the result of changes in the relative strength of the two modes. It has in no case proved possible to investigate this question directly, however.

VI. CONCLUSIONS

We summarize the main results of this paper as follows. Radiation is emitted by the pulsar as an admixture of two orthogonal modes of polarization such that the resultant state of polarization can be described by

$$I = I_1 + I_2 + I_{\rm unpol}\,, \tag{13}$$

$$V = V_1 + V_2 = d_{V_1} I_1 - d_{V_2} I_2\,, \tag{14}$$

$$L = L_1 + L_2 = (d_{L_1} I_1 - d_{L_2} I_2) \exp(2i\psi)\,, \tag{15}$$

where $\psi(\phi)$ varies slowly with longitude ϕ. The two modes are manifested by opposite signs of circular polarization and position angles that are 90° apart. In other words, the modes correspond to two positions on the Poincaré sphere that lie on a great circle that passes through the north and south poles. If the two modes are of equal ellipticity, then they are connected by a diameter of the Poincaré sphere as well. At large radio frequencies (e.g., at least ~1 GHz) an additional polarized component of emission contributes which is different from and apparently dominates the orthogonal-mode emission (Manchester, Taylor, and Huguenin 1975).

The state of polarization, like the intensity, is extremely variable, so that all quantities in equations (13)–(15) [except $\psi(\phi)$] should be regarded as stochastic. We have confirmed the accuracy of the above equations for PSR 2020+28 by demonstrating that the sign of circular polarization is highly correlated with the sign of the quantity $L \exp(-2i\psi)$. PSR 2020+28 was appropriate for this demonstration because emission at any instant often appears to be in only one mode. Emission from PSR 1133+16 and PSR 2016+28 (Cordes and Hankins 1977), however, is apparently a superposition of the modes, because the correlation between V and $L \exp(-2i\psi)$ is not as well defined. Cordes and Hankins found for PSR 1133+16 that a sign change of circular polarization was a necessary but not a sufficient occurrence in order to predict a 90° change in position angle. While a sign change of V in the absence of a position-angle jump may represent a significant counterexample to our generalizations, it is more likely to be a consequence of the statistical variability of the quantities $I_{1,2}$, $d_{V_{1,2}}$, and $d_{L_{1,2}}$, in equations (14) and (15). That is, given I_1 and I_2, the quantities d_{V_1} and d_{V_2} can change so as to effect a sign change of V, while d_{L_1} and d_{L_2} may have values such that the position angle remains unchanged.

As for the dynamics by which the state of polarization changes between modes (mode transitions), PSR 2020+28 indicates that transitions are dependent on intensity. In single pulses, transitions occur on the trailing edges of subpulses in component I or where saddle region emission and component I emission overlap. In component II, one mode is clearly associated with a larger range of intensities than the other mode. However, peak subpulse emission can be in either of the modes, and sometimes transitions between modes do not occur on the edges of subpulses. Therefore, although mode transitions preferentially occur on subpulse edges, their occurrence is stochastic, perhaps indicating the untenability of a geometric interpretation of the transitions as aspects of an angular beam of radiation.

The phenomenology of modes of polarization is so far consistent with a mechanism that generates pulselike emission such that the strengths of the two modes become comparable on the periphery of the pulselike feature. Observed subpulse (and micropulse) emission can be formed in two ways: as a temporal modulation of an emission region, or as a subbeam of emission that is swept across the line of sight. The distinction between angular beaming and temporal modulation in the context of the polar-cap model is treated in some detail by Cordes, Rickett, and Hankins (1978). In either case, the periphery of the pulse is associated with some spatial boundary of the emission region or with a particular aspect in the evolution of the emission region when it is beginning or terminating its role as a coherent emitter. It becomes tempting to associate

mode switching with the details of the radiative transfer of two modes of polarization that are intrinsic to the radiation process. It seems likely that radiative transfer will be qualitatively different at peak radiation and at the edges of a pulse if those edges are indeed related to a spatial or temporal boundary.

We thank T. H. Hankins and D. B. Campbell for help with the observations, E. Tademaru and P. Backus for helpful discussions, and Ginny O'Connor and Annie Smith for preparing the manuscript. This research was supported by the National Science Foundation through grant MPS 75-03377. Arecibo Observatory is operated by Cornell University under contract to the NSF. This is Contribution 252 of the Five College Observatory.

REFERENCES

Backer, D. C. 1976, *Ap. J.*, **209**, 895.
Backer, D. C., Rankin, J. M., and Campbell, D. B. 1975, *Ap. J.*, **197**, 481.
———. 1976, *Nature*, **263**, 202.
Blandford, R. D., and Scharlemann, E. T. 1976, *M.N.R.A.S.*, **174**, 59.
Cordes, J. M. 1975, *Ap. J.*, **195**, 193.
———. 1976*a*, *Ap. J.*, **208**, 944.
———. 1976*b*, *Ap. J.*, **210**, 780.
Cordes, J. M., and Hankins, T. H. 1977, *Ap. J.*, **218**, 484.
Cordes, J. M., Rickett, B. J., and Hankins, T. H. 1978, in preparation.
Hankins, T. H. 1971, *Ap. J.*, **169**, 487.
———. 1972, *Ap. J.* (*Letters*), **177**, L11.
———. 1973, *Ap. J.* (*Letters*), **181**, L49.
Helfand, D. J., Manchester, R. N., and Taylor, J. H. 1975, *Ap. J.*, **198**, 661.
Huguenin, G. R., Taylor, J. H., and Helfand, D. J. 1973, *Ap. J.* (*Letters*), **181**, L139.
Komesaroff, M. M. 1970, *Nature*, **225**, 612.
Manchester, R. N., and Taylor, J. H. 1977, *Pulsars* (San Francisco: Freeman), p. 220.
Manchester, R. N., Taylor, J. H., and Huguenin, G. R. 1975, *Ap. J.*, **196**, 83.
Radhakrishnan, V., and Cooke, D. J. 1969, *Ap. Letters*, **3**, 225.
Rankin, J. M., Campbell, D. B., and Backer, D. C. 1974, *Ap. J.*, **188**, 609.
Rankin, J. M., Campbell, D., and Spangler, S. 1975, NAIC Rept. 46.
Rickett, B. J., Hankins, T. H., and Cordes, J. M. 1975, *Ap. J.*, **201**, 425.
Taylor, J. H., Huguenin, G. R., Hirsch, R. M., and Manchester, R. N. 1971, *Ap. Letters*, **9**, 205.

D. C. Backer: Radio Astronomy Laboratory, University of California, Campbell Hall, Berkeley, CA 94720

J. M. Cordes: Department of Physics and Astronomy, GRC Tower B, University of Massachusetts, Amherst, MA 01003

Joanna Rankin: Astronomy Department, Cornell University, Ithaca, NY 14853

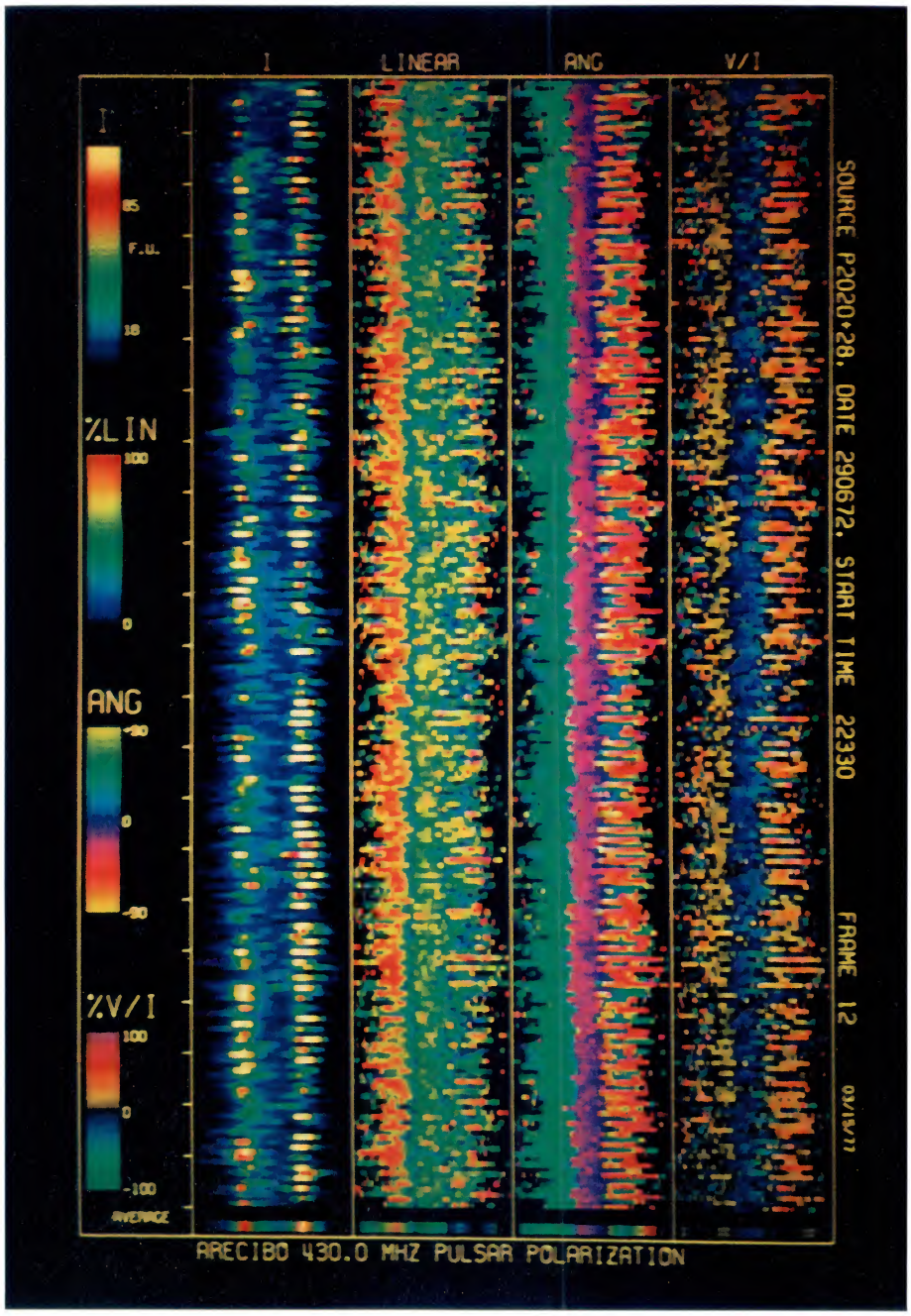

FIG. 1.—Color intensity–coded display of the individual pulse polarization properties of a sequence of 220 pulses from pulsar PSR 2020+28 at 430 MHz on 1972 June 29; average values for the sequence are given at the very bottom of the display. A total longitude interval of 28°.3 is plotted. The four columns are the total intensity, "*I*"; percentage linear polarization, "LINEAR"; the polarization angle, "ANG"; and the percentage circular polarization, "*V*/*I*."

CORDES *et al.* (*see* page 962).